JOURNAL OF GUIDANCE, CONTROL, AND DYNAMICS
Vol. 33, No. 2, March–April 2010

Endgame Problem Part 1: V_∞-Leveraging Technique and the Leveraging Graph

Stefano Campagnola*
University of Southern California, Los Angeles, California 90089-1191
and
Ryan P. Russell†
Georgia Institute of Technology, Atlanta, Georgia 30332-0150

DOI: 10.2514/1.44258

Renewed interest by ESA and NASA in missions to Europa, Ganymede, Enceladus, and Titan poses the question of how to best solve the endgame problem. Endgames typically aim at an inexpensive insertion maneuver into the science orbit and can be designed using either V_∞-leveraging maneuvers or the multibody dynamics. Although historically linked to insertion maneuvers, the endgame problem is symmetric and equally applies to departure. In this two-part series, we analyze and draw connections between the two apparently separate approaches, providing insight into the dynamics of the multibody gravity-assist problem. In this paper we derive new formulas for the V_∞-leveraging maneuver and build the leveraging graph to be used as a reference guide for designing endgame tours. We prove that the cost of a V_∞-leveraging-maneuver sequence decreases when using high-altitude flybys (as done in the multibody technique). Finally, we find a simple quadrature formula to compute the minimum ΔV transfer between moons using V_∞-leveraging maneuvers, which is the main result of the paper, and a method to estimate transfer times. The leveraging graphs and associated formulas are derived in canonical units and therefore apply to any celestial system with a smaller body in a circular orbit around a primary. Specifically, we demonstrate the new method to provide rapid calculations of the theoretical boundary values for ΔV requirements and estimated transfer times for moon tours in the Saturn and Jupiter systems using the V_∞-leveraging-maneuver model.

Nomenclature

A = point in arc L–A at which the impulsive maneuver takes place
a_M = semimajor axis of the minor body (1 in nondimensional units)
B = point in arc H–B at which the impulsive maneuver takes place
H = point in arc H–B at which the spacecraft orbit crosses the minor-body orbit
h_π = altitude of the spacecraft's closest approach to the minor body
K = number of full revolutions in arc H–B
L = point arc L–A at which the spacecraft orbit is tangent to the minor-body orbit with a low relative velocity $V_{\infty L}$
m = number of spacecraft revolutions
n = number of moon revolutions
r_A = distance from point A to the major body
r_M = radius of the minor body
V_c = velocity of the spacecraft at a circular orbit with altitude h_π around a moon with gravitational parameter μ_M
V_M = velocity of the minor body with respect to the major body (1 in nondimensional units)
V_π = velocity of the spacecraft with respect to the minor body at the pericenter of the hyperbola
V_∞ = relative velocity of the spacecraft at the minor body
$V_{\infty H}$ = velocity of the spacecraft relative to the minor body at point H
$V_{\infty L}$ = velocity of the spacecraft relative to the minor body at point L
ΔV_{AB} = impulsive maneuver at point A, B
μ = gravitational parameter
$\pm$ = exterior/interior V_∞-leveraging maneuvers
$\sim$ = dimensional variable

Subscripts

M = minor body
P = major body

Superscripts

E = exterior V_∞-leveraging maneuver
I = interior V_∞-leveraging maneuver
$\pm$ = long/short transfer

Introduction

IN RECENT years both NASA and ESA have studied a variety of mission options to the Galilean moons at Jupiter and to the moons of Saturn, including Enceladus and Titan. A very challenging part of the trajectory design of these missions is the endgame [1], the last part of the tour before the insertion maneuver into the science orbit. The endgame aims at a low-ΔV orbit-insertion maneuver. The begin-game is the symmetric problem and starts with a low-ΔV escape from an initial orbit around a minor body. Both strategies have been studied, designed, and implemented in space missions with two distinct approaches.

The first approach uses the V_∞-leveraging-maneuver (VILM) technique, in which the combined effect of gravity assists and impulsive maneuvers (at the almost opposite apsidal point of the

Presented at the AIAA/AAS Space Flight Mechanics Meeting, Savannah, GA, 8–12 February 2020; received 20 April 2009; revision received 2 November 2009; accepted for publication 2 November 2009.

*Ph.D. Student, Aerospace and Mechanical Engineering, 854 Downay Way; stefano.campagnola@missionanalysis.org. Member AIAA.
†Assistant Professor, Guggenheim School of Aerospace Engineering, 270 Ferst Drive; ryan.russell@gatech.edu. Member AIAA.

spacecraft orbit) changes the spacecraft velocity relative to the minor body [2,3]. Typically, the transfer is first computed in the linked-conics model (i.e., the zero-sphere-of-influence patched-conics model) and then optimized in a real ephemeris model and patched together to the rest of the trajectory. The VILM approach is very intuitive and quickly provides solutions. NASA and ESA use the VILM approach for the design of the endgame trajectories to Europa [1,4], Ganymede [5], and Titan. The VILM originates and is used frequently with interplanetary trajectories [2,3]. The Messenger mission to Mercury implements a VILM sequence for the endgame at Mercury [6]; the BepiColombo mission to Mercury implements a low-thrust version of the VILM at Earth and at Mercury [7], followed by a gravitational capture at Mercury [8]. The Cassini spacecraft performed a VILM at Venus before the last Earth gravity assist [9]. The Juno mission, targeted to launch in 2011, implements a VILM at Earth to reach Jupiter [10].

The second approach uses the multibody technique [11,12] in which small ΔV (if any) are applied when the spacecraft is far from the minor body, typically to target high-altitude flyby passages that produce the desired effects (e.g., behind or in front of the minor body to increase or decrease the spacecraft energy). The trajectory is computed directly in the real ephemeris model, or in the restricted three-, four-, or five-body model. This approach cannot be explained with the linked-conics model, in which ballistic transfers cannot change the arrival conditions at the minor body. Trajectories are typically found with some heuristic method. Recently, nonlinear dynamical system theory has been used to help the design of endgames or multimoon orbiters [4,13]. The multibody technique usually results in low-cost trajectories with long times of flight. The SMART-1 mission successfully implemented this strategy to get the spacecraft gravitationally captured around the moon [12].

In this two-part series, we study the endgame transfers in general and show the connections between the two approaches. The first part of the work, presented in this paper, studies the anatomy of the VILM. In the first section we derive formulas to show that VILMs are efficient only for V_∞ greater than a minimum value. In the second section we use the formulas to introduce the leveraging graph, which has broad endgame design applications. Based on the graph, we demonstrate a branch-and-bound search to globally explore the flight time vs ΔV solution space. The canonical form of the leveraging graphs and formulas are applicable to any planet system or moon system modeled as a smaller body in a circular orbit around a primary. A simple scaling transforms the problem to any dimensioned system of interest. In the third section we define and study the efficiency of the VILM. We prove that the cost of a sequence of VILMs decreases when using high-altitude gravity assists (as done when using the multibody technique). Finally, we find the theoretical minimum ΔV for transfer between moons computed using the VILM approach. This new design capability is the main result of the paper.

In the second part of this work [14], we will focus on the multibody technique and will explain the connection to the VILM approach.

V_∞-Leveraging

A VILM is a technique by which a spacecraft orbiting around a major body P can change its speed relative to a minor body M [2,3]. The technique consists of a gravity assist and a small impulsive maneuver ΔV_{AB} that occurs at opposite apses in the spacecraft orbit around the major body (see Fig. 1) . VILMs are typically modeled in the linked-conics model (or zero-sphere-of-influence patched-conics model), in which the minor body is considered massless and is on a circular orbit around the major body. The spacecraft trajectory is coplanar and starts and ends at the minor body. The gravity assist is modeled as an instantaneous change in the direction of the V_∞ vector by angle δ.

Nondimensional Variables

Throughout this work we will use nondimensional variables so that the results are general and can be applied to any endgame problem. To obtain the nondimensional variables, we divide the dimensional variable (denoted with the tilde) by the time and length scale factors:

$$l_{\text{scale}} = \tilde{a}_M, \qquad t_{\text{scale}} = \sqrt{\frac{\tilde{a}_M^3}{\tilde{\mu}_P}}$$

Then the velocity scale factor becomes the velocity of the minor body $\tilde{V}_M$, and the nondimensional velocity, the semimajor axis of the minor body, and the gravitational parameter of the major body are one.

We also define V_c as the nondimensional velocity of the circular orbit of radius $\tilde{r}_\pi = \tilde{r}_M + \tilde{h}_\pi$ around the minor body:

$$V_c = \sqrt{\frac{\tilde{\mu}_M}{\tilde{r}_\pi}} \Big/ \tilde{V}_M$$

This nondimensional parameter groups the problem dependency on the minor-body gravitational parameter, minor-body radius, and altitude of the final/initial orbit-insertion/escape.

In nondimensional units, the gravity-assist deflection angle is

$$\delta = 2 \arcsin(1/[1 + (V_\infty/V_c)^2])$$

and the spacecraft velocity at the closest approach to the minor body, V_π, is

$$V_\pi(V_\infty, h_\pi) = \sqrt{V_\infty^2 + 2V_c^2} \tag{1}$$

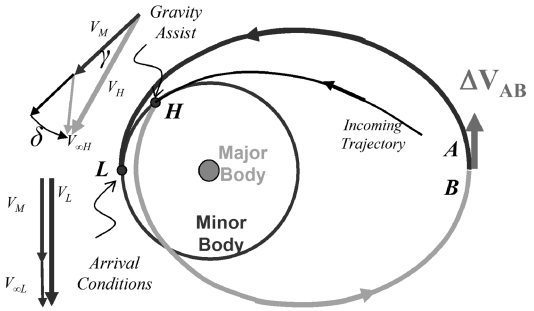

Fig. 1 Example of a VILM to reduce the relative velocity at a minor body: The spacecraft approaches the minor body tangentially and the gravity assist at H rotates the relative velocity $V_{\infty H}$ of an angle δ. At the apocenter of the new orbit (point B), the impulsive maneuver ΔV_{AB} changes the shape of the spacecraft orbit so that it becomes tangent again to the minor-body orbit at point L. Although the maneuver actually increases the spacecraft energy, at point L the spacecraft has a new relative velocity $V_{\infty L} < V_{\infty H}$.

VILM Model and Classification

In this section we refer to Figs. 2 and 3 to define the general variations and associated relevant variables of the VILM. We assume that the impulsive maneuver is tangential and is performed exactly at the apses. This assumption is typically included when studying VILMs, because the Jacobi constant in the rotating frame is maximally changed by performing the maneuver when the rotating velocity is the greatest, which occurs at apses [15]. We also assume that the spacecraft departs/arrives at point L tangent to the minor-body orbit. This condition guarantees the lowest $V_{\infty L}$ [16] and greatly simplifies the tour problem, because we can decouple each VILM as opposed to having to optimize a large sequence of VILMs altogether.

We divide the trajectory into two legs (A–L and B–H) joining four different states of the spacecraft (L, A, B, and H). At point L the spacecraft is at an apse with a relative velocity $V_{\infty L}$ with respect to the minor body. At point A the spacecraft is at the opposite apsidal point, at a distance r_A from the major body and with a velocity V_A. Between states A and B, the spacecraft performs the impulsive maneuver

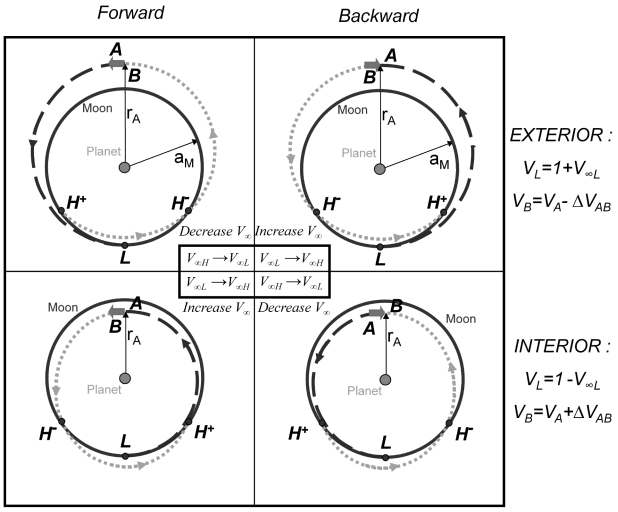

Fig. 2 Four variations of the VILM.

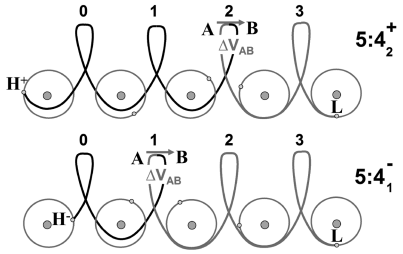

Fig. 3 Schematic of two different 5:4 VILMs. In one case the ΔV_{AB} occurs after two full revolutions of the spacecraft on the leg H^+–B. Also, the transfer lasts a bit more than five revolutions of the minor body; hence the notation 5:4$_2^+$. In the other case the ΔV_{AB} occurs after one full revolution of the spacecraft on the leg H^-–B. Also, the transfer lasts a bit less than five revolutions of the minor body; hence the notation 5:4$_1^-$.

$\Delta V_{AB} = |V_A - V_B|$. At point H^+ or H^-, the spacecraft intersects the minor-body orbit with a relative velocity $V_{\infty H} > V_{\infty L}$.

We recall from the literature [3] that there are four types of V_∞-leveraging maneuvers, depending on the following features:

1) The VLM is called forward (backward) if the ΔV_{AB} is in the same (opposite) direction of the spacecraft velocity.

2) The VLM is called exterior (interior) if the ΔV_{AB} occurs at apocenter (pericenter), thus if $r_A > a_M$ ($r_A < a_M$).

From these definitions it follows that the forward exterior V_∞-leveraging and backward interior V_∞-leveraging *decrease* the V_∞, whereas the forward interior V_∞-leveraging and backward exterior V_∞-leveraging increase the V_∞.

From our definitions it also follows that

$$V_L^{(E,I)} = 1 \pm V_{\infty L} \tag{2}$$

$$V_A^{(E,I)} = V_B \pm \Delta V_{AB} \tag{3}$$

where the upper sign refers to the exterior VILM and the lower sign refers to the interior VILM. Note that from these definitions and from Fig. 2, we find boundary values for V_∞. In particular, $0 < V_{\infty L} < \sqrt{2} - 1$ for the exterior VILM for r_A to be bounded, and $0 < V_{\infty L} < 1$ for the interior VILM for V_L to be positive.

For each type of VILM, we also specify the following:

1) The resonant ratio is n:m, where n (m) is the approximate number of the minor-body (spacecraft) revolutions during the VILM.

2) K is the number of full revolutions in the arc H–B. [In the literature we can find a different choice of letters: K:$L(M)^{\pm}$, where $K \equiv n$, $L \equiv m$, and $M \equiv K$ for exterior VILM.]

3) The point H^- or H^+ at which the spacecraft encounters the minor body results in a *long-transfer* VILM or *short-transfer* VILM, respectively. Exterior long-transfer VILMs and interior short-transfer VILMs are linked by prograde gravity assists. Exterior short-transfer VILMs and interior long-transfer VILMs are linked by retrograde gravity assists.

As an example, Fig. 3 shows the schematic of a 5:4$^+$ and a 5:4$^-$ VILM. In the rest of the paper, we refer to backward/forward interior/exterior n:$m_K^{\pm}$ VILMs. For example, the Europa endgame when approached from Ganymede is a sequence of forward exterior VILMs.

Phase-Free Formulas

In this section we present a general formulation that is valid for all four types of VILM. We start by considering the phase-free problem that does not require the spacecraft and the minor body to be at points L and $H^{\pm}$ at the same time. The formulas presented in this section are new and allow us to perform many useful, fast, preliminary, and global analyses, which we present in the next sections. The details of the following calculations are in Appendix A.

We first define the function

$$\Gamma^{(E,I)}(V_{\infty L}) \equiv \pm(r_A - V_A) = V_{\infty L}\frac{V_{\infty L}^3 \pm 3V_{\infty L}^2 - V_{\infty L} \mp 7}{V_{\infty L}^3 \pm 3V_{\infty L}^2 + V_{\infty L} \mp 1}$$

where $\Gamma^{(E)}$ is computed for the exterior VILM, and $\Gamma^{(I)}$ is computed for the interior VILM. If no distinction is necessary, we simply refer to Γ. We can show that Γ is a positive strictly monotonic function of V_∞. Later, we will see that Γ is convenient because it provides a minimum bound on V_∞ values at which VILMs are useful.

With this notation we can explicitly state the high relative velocity $V_{\infty H}$ as a function of the low relative velocity $V_{\infty L}$ and of the ΔV_{AB}:

$$V_{\infty H}(V_{\infty L}, \Delta V_{AB}) = \sqrt{(V_{\infty L})^2 + (\Delta V_{AB})^2 + 2\Delta V_{AB}\Gamma} \tag{4}$$

Equivalently, we can explicitly state the ΔV_{AB} as a function of the high and low relative velocity:

$$\Delta V_{AB}(V_{\infty L}, V_{\infty H}) = -\Gamma + \sqrt{\Gamma^2 + (V_{\infty H}^2 - V_{\infty L}^2)} \tag{5}$$

Finally, we define the *phase-free efficiency* of the VILM. The phase-free efficiency of backward interior or forward exterior VILM ϵ_{BI-FE} is the increase of the final relative velocity $V_{\infty H}$, due to a change in cost ΔV_{AB}, for a fixed initial relative velocity $V_{\infty L}$:

$$\epsilon_{BI-FE} \equiv \frac{\partial V_{\infty H}}{\partial \Delta V_{AB}} \equiv D_2 V_{\infty H} = \frac{\Delta V_{AB} + \Gamma}{V_{\infty H}(V_{\infty L}, \Delta V_{AB})} \tag{6}$$

where D_i is the derivative with respect to the ith argument. The phase-free efficiency of backward exterior or forward interior VILMs ϵ_{BE-FI} is the decrease of the final relative velocity $V_{\infty L}$, due to a change in cost ΔV_{AB}, for a fixed initial relative velocity $V_{\infty H}$:

$$\epsilon_{BE-FI} \equiv -\frac{\partial V_{\infty L}}{\partial \Delta V_{AB}}$$

We derive an expression for ϵ_{BE-FI} by first taking the partial derivative of $V_{\infty H}$ with respect to $V_{\infty L}$:

$$D_1 V_{\infty H} \equiv \frac{\partial V_{\infty H}}{\partial V_{\infty L}} = \frac{V_{\infty L} + \Delta V_{AB}(\mathrm{d}\Gamma/\mathrm{d}V_{\infty L})}{V_{\infty H}(V_{\infty L}, \Delta V_{AB})} \tag{7}$$

We then use the implicit function theorem [17] to compute

$$\epsilon_{BE-FI} = -\frac{\partial V_{\infty L}}{\partial \Delta V_{AB}} = D_2 V_{\infty H} \circ [D_1 V_{\infty H}]^{-1} = \frac{\Delta V_{AB} + \Gamma}{V_{\infty L} + \Delta V_{AB}(\mathrm{d}\Gamma/\mathrm{d}V_{\infty L})} \tag{8}$$

Phase-Fixed Solutions

In this section we restore the phasing constraint and introduce the concept of leveraging graphs. A numerical solution to this constrained problem can be computed using an algorithm described by

Sims et al. [3]. In general, given $V_{\infty H}$, the steps of the algorithm are the following:

1) We assume the minor body and the spacecraft are both at point H at time t_H.

2) We guess the flight-path angle γ at H (see Fig. 1) and find the orbital parameters of the leg H–B.

3) We compute the orbital parameters of the leg L–A with apses at L and r_A.

4) We compute the transfer time and the time t_L when the spacecraft is at L.

5) We compute the distance from point L to the position of the minor body at time t_L and differentially correct the flight-path angle γ until the distance vanishes.

The numerical solutions to the VILM problem are one set of $V_{\infty H}$ ($V_{\infty L}$) curves for exterior $n{:}m_K^{\pm}$ VILMs and one set of $V_{\infty H}$ ($V_{\infty L}$) curves for the interior $n{:}m_K^{\pm}$ VILMs. We plot these solutions on a special graph, which we call the $V_{\infty L}$–$V_{\infty H}$ *leveraging graph.* We can also plot these solutions using other variables related to V_∞, thus defining different leveraging graphs. In the next section we build and use the *Tisserand leveraging graph.* Following this definition, the graphs in the literature can be referred to as r_{aphelion}–$V_{\infty\text{Earth}}$ leveraging graphs or (r_{aphelion}–ΔV_{TOT}) leveraging graph etc. [2,3].

Figure 4 shows the $V_{\infty L}$–$V_{\infty H}$ leveraging graphs for the exterior (Fig. 4a) and interior (Fig. 4b) VILM (the domain of feasible $V_{\infty L}$ is discussed in the previous section). In these graphs, for simplicity and clarity, we plot only one VILM (the most efficient) for each $n{:}m$ case.

We emphasize that the leveraging maneuvers and graphs are computed only once in nondimensional units so that they can be applied to any endgame problem using the scale factors. Note that all of the numerical solutions presented in Fig. 5 are computed using a 200-line code written in MATLAB. The computational time is approximately 1 min using a dual-core 1.83 GHz laptop processor.

Figure 5 shows a close-up of the exterior (Fig. 5a) and interior (Fig. 5b) VILM. In contrast to Fig. 4, all VILM solutions are plotted for each $n{:}m$ case. As an example, we show that the 3:2 exterior VILM reduces the V_∞ from $V_{\infty H} = 0.131$ to $V_{\infty L} = 0.1135$. By plotting the level sets of the phase-free function $\Delta V_{AB}(V_{\infty L}, V_{\infty H})$ of Eq. (5) we estimate the $\Delta V_{AB} \approx 0.0022$. For a VILM at Europa, we multiply these values by the average velocity of Europa of approximately 13.7 km/s to find that we decrease $\tilde{V}_{\infty H} = 1.8$ km/s to $\tilde{V}_{\infty L} = 1.56$ km/s using approximately 30 m/s.

Finally, we define the phase-fixed efficiency E of the VILM as the ratio between the variation of V_∞ and the ΔV_{AB}:

$$E = \frac{V_{\infty H} - V_{\infty L}}{\Delta V_{AB}}$$

Figure 6 shows the phase-fixed efficiency of the exterior (Fig. 6a) and interior (Fig. 6b) VILM. The figure shows that the most efficient VILMs are those with the largest possible value of K ($K_{\text{best}} = m - 1$) and longest transfer time. However, we avoid discarding the less

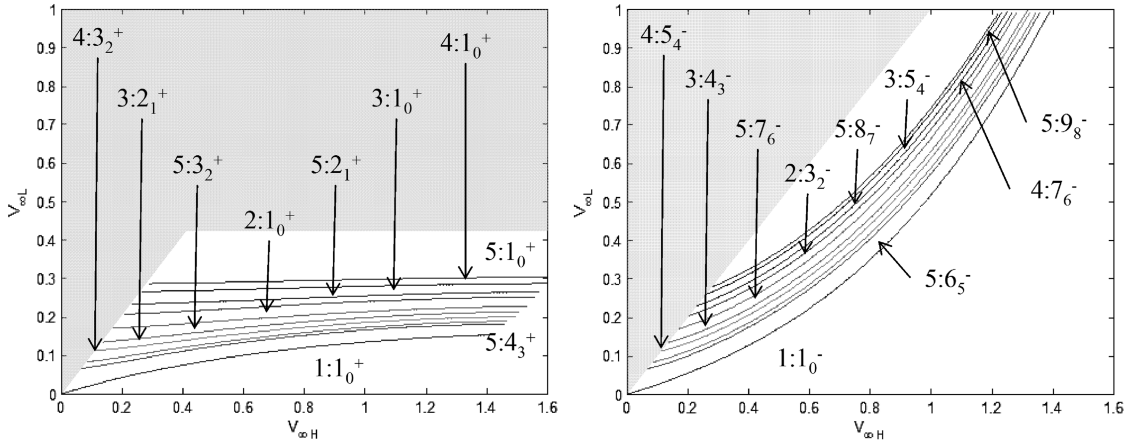

Fig. 4 $V_{\infty L}$–$V_{\infty H}$-leveraging graph for the a) exterior and b) interior VILM. For each resonance $n{:}m$ we only plot the VILM $n{:}m_{m-1}^+$, which we show to be the most efficient. The domain of feasible $V_{\infty L}$ is discussed in the previous section.

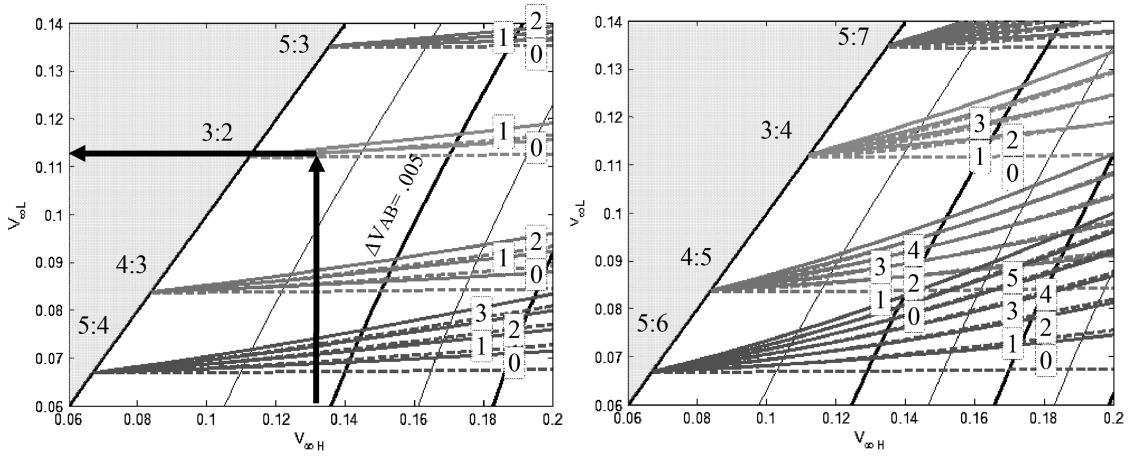

Fig. 5 $V_{\infty L}$–$V_{\infty H}$-leveraging graph for the exterior a) exterior and b) interior VILM. In these close-ups,we plot $2m$ curves for each $n{:}m$ resonance. The dashed curves are the short-transfer VILMs (one dashed curve for each K, $0 < K < m - 1$). The solid curves are the long-transfer VILMs (one solid curve for each K, $0 < K < m - 1$). The K parameter is indicated in the box. We also plot contour lines representing constant-ΔV_{AB}.

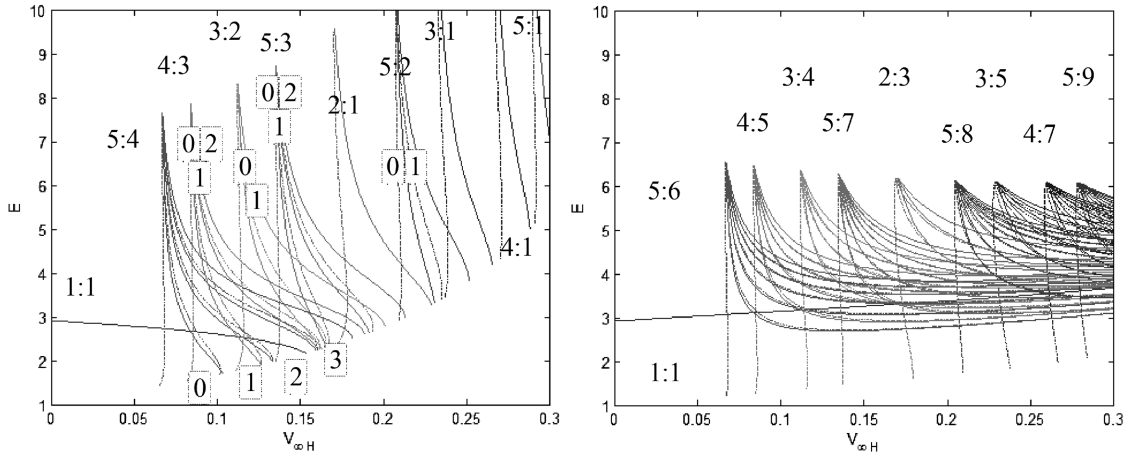

Fig. 6 Efficiency of the a) exterior and b) interior VILM. The dashed curves are the short-transfer VILMs, while the solid curves are the long-transfer VILMs. The numbers in the boxes represent the values of the parameter *K*. For any given resonance *n*:*m*, the most efficient VILM is $n{:}m^{+}_{m-1}$.

efficient solutions, because the difference in efficiency can often be compensated when computing the VILM in more accurate models.

Minimum $V_{\infty L}$

In the previous example we showed that a ΔV_{AB} of approximately 30 m/s reduces the relative velocity by approximately 240 m/s. However, it is not always true that the ΔV_{AB} is smaller than the actual gain/loss in relative velocity magnitude at the flyby body. In what follows we show that this occurs only if $V_{\infty L}$ is larger than a given value, which depends on V_c.

Let us assume an endgame problem in which the spacecraft initially approaches the minor body with $V_{\infty H}$. The spacecraft needs $\Delta V_{\pi H} = V_{\pi H} - V_c$ to be captured in the target orbit. Alternatively, the spacecraft can perform a VILM that reduces the relative velocity to $V_{\infty L}$, and the new orbit-insertion maneuver requires $\Delta V_{\pi L} = V_{\pi L} - V_c$. Then the VILM is efficient as long as the reduction of V_π is greater than the VILM cost ΔV_{AB}.

Proposition: The VILM strategy is efficient if $V_{\infty L} > \bar{V}_\infty$, where $\bar{V}_\infty = \sqrt{\bar{V}_\pi^2 - 2V_c^2}$ and $\bar{V}_\pi(V_c)$ is the root of the function

$$f(V_\pi) = \Gamma \circ V_\infty(V_\pi; V_c) - V_\pi \tag{9}$$

where V_c is a parameter for f, and $\circ$ denotes function composition.

Proof: From Eq. (1) we find

$$V_{\infty H}^2 = V_{\pi H}^2 - 2V_c^2, \qquad V_{\infty L}^2 = V_{\pi L}^2 - 2V_c^2 \tag{10}$$

We square Eq. (4) and use Eq. (10) to find

$$(V_{\pi H})^2 = (V_{\pi L} + \Delta V_{AB})^2 + 2\Delta V_{AB}(\Gamma - V_{\pi L})$$

The VILM strategy is efficient if ΔV_{AB} is less than the change in V_π: thus, if

$$V_{\pi H} > (V_{\pi L} + \Delta V_{AB}) \rightarrow \Gamma - V_{\pi L} > 0$$

To solve the problem we need to study the function

$$f(V_{\pi L}) = \Gamma \circ V_\infty(V_{\pi L}; V_c) - V_{\pi L}$$

where V_c is a parameter.

For $V_{\pi L} = \sqrt{2}V_c$, we have $V_{\infty L} = \Gamma = 0$, thus $f(\sqrt{2}V_c) = -V_c$. Also,

$$\frac{\mathrm{d}f}{\mathrm{d}V_\pi} = \frac{\mathrm{d}\Gamma}{\mathrm{d}V_{\infty L}} \times \frac{V_{\pi L}}{V_{\infty L}} - 1 > 0$$

(An expression for $\mathrm{d}\Gamma/\mathrm{d}V_{\infty L}$ is given in Appendix A.) Then $f(V_\pi) > 0$ if $V > \bar{V}_\pi$, where $\bar{V}_\pi(V_c)$ is the only root of $f(V_\pi) = 0$. Note that the root for the exterior VILM is different from the root of the interior VILM, as $\Gamma^{(E)} \neq \Gamma^{(I)}$.

To compute $\bar{V}_\pi$ we numerically find the root of the function in Eq. (9). Then we use Eq. (1) to find $\bar{V}_\infty$. $\bar{V}_\infty$ as a function of the parameter V_C for the exterior and interior case can be approximated by the following cubic splines:

$$\begin{aligned}
\bar{V}_\infty^E &= +(5.9561662273454\mathrm{e}-5)V_c^3 \\
&\quad -(5.1344907043886\mathrm{e}-2)V_c^2 \\
&\quad +(2.0441849005940\mathrm{e}-1)V_c \\
&\quad -(7.2712278793706\mathrm{e}-6) \\
\bar{V}_\infty^I &= -(1.9176499488104\mathrm{e}-2)V_c^3 \\
&\quad +(5.1814140491440\mathrm{e}-2)V_c^2 \\
&\quad +(2.0377335047117\mathrm{e}-1)V_c \\
&\quad +(8.7463066767540\mathrm{e}-6)
\end{aligned}$$

Leveraging Graph and the Europa Endgame

Tisserand Leveraging Graph

In this section we introduce the Tisserand leveraging graph, which we use to design endgame strategies. The Tisserand graph is a graph representing the pericenter r_p and period T of a Keplerian coplanar orbit around a major body [18,19]. Certain points (r_p and T) on the graph represent orbits that intersect the orbits of minor bodies of the system. For these points we can compute V_∞ with respect to the minor bodies that the given orbits intersect. We can then populate the Tisserand graphs with a set of V_∞ level sets for each minor body. When a spacecraft performs a gravity assist at one minor body, it changes its location on the graph while staying on the V_∞ level set. For this reason, the Tisserand graph is a useful graph of the planetary/moon systems and it has been used to design complicated multiple gravity-assist trajectories [16,20,21].

The Tisserand leveraging graph is an extension of the Tisserand graph, which includes the numerical solutions of the VILM. Because we use nondimensional units, we need only compute the graph once and then scale it for the different minor bodies we want to include. To build the graph, we begin by computing the Tisserand graph [18,19] and representing it with the apocenter on the x axis and the pericenter on the y axis. This choice of the axes results in rectangular semi-infinite subdomains of the minor bodies and in period level sets that are straight diagonal lines with a slope of -1. Starting with a r_a–r_p orbit, the new r_a–r_p following a VILM is aligned horizontally or vertically with the initial state, as follows:

1) The ΔV_{AB} of the interior VILM changes the apocenter but not the pericenter of the initial orbit. We represent the interior VILM with a horizontal shift from/to the line $r_a = 1$.

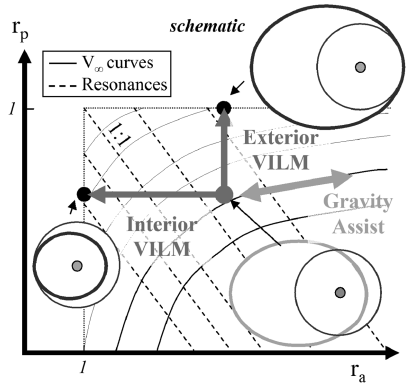

Fig. 7 Schematic apocenter–pericenter Tisserand graph and the effect of an interior and exterior VILM. We also plot the period level sets and the V_∞ level sets. A gravity assist moves the spacecraft r_a–r_p along the V_∞ level set. The VILM ΔV_{AB} moves the spacecraft r_a–r_p horizontally or vertically, thus changing the V_∞.

2) The ΔV_{AB} of the exterior VILM changes the pericenter but not the apocenter of the spacecraft orbit. We represent the exterior VILM with a vertical shift from/to the line $r_p = 1$.

In Fig. 7 we show a schematic Tisserand graph. We use the apocenter–pericenter representation and show the effect of an interior and exterior VILM. We also plot the period level sets, V_∞ level sets, and the effect of a gravity assist. We clearly see how the ΔV_{AB} changes the V_∞.

We proceed by including the numerical solutions of the VILM. We plot the curves in Fig. 4 onto the Tisserand graph, and we obtain the Tisserand leveraging graph. Figure 8 shows the Tisserand leveraging graph in nondimensional units. We only include the VILMs with $K = m - 1$, as we showed in the previous section they are the most efficient. The solid thick lines are the long-transfer VILMs, and the dotted thick lines are the short-transfer VILMs.

Endgame at Europa Using the Tisserand Leveraging Graph

In this section we use the Tisserand leveraging graph to design Europa endgames starting at $\tilde{V}_{\infty\text{initial}} = 1.8$ km/s (1.8 km/s is slightly above the $\tilde{V}_\infty$ that can be achieved by multiple gravity assists only [16,22]). We assume that the endgame consists of a series of forward exterior VILMs. We first design one single endgame and then apply the same design strategy in a branch-and-bound search, storing the total time of flight (ToF) and the total $\Delta\tilde{V}_{\text{TOT}}$:

$$\Delta\tilde{V}_{\text{TOT}} = \sum_i (\Delta\tilde{V}_{AB})_i + \Delta\tilde{V}_{\pi\text{EOI}}$$

where $\Delta V_{\pi\text{EOI}}$ is the Europa orbit-insertion maneuver

$$\Delta\tilde{V}_{\pi\text{EOI}} = \tilde{V}_\pi(\tilde{V}_{\infty\text{final}}, \tilde{h}_\pi) - \tilde{V}_c$$

We start designing one Europa endgame, which is a sequence of forward interior VILMs. Figure 9 is a close-up of the Tisserand leveraging graph scaled to Europa by multiplying the distances by the semimajor axis of the Europa orbit and by multiplying the velocities by the velocity of Europa. We also plot the level sets of the function $\Delta\tilde{V}_{AB}(\tilde{V}_{\infty L}, \tilde{V}_{\infty H})$ in Eq. (5). The starting point of the endgame is point A on the figure. The first VILM is composed of a gravity assist and a $(\Delta\tilde{V}_{AB})_1$. During the gravity assist, the spacecraft moves along the $\tilde{V}_\infty = 1.8$ km/s level set until it intersects, for example, the $3{:}2^+_1$ curve (point B). Then the $\Delta\tilde{V}_{AB}$ at apocenter raises the pericenter to a_M (point C). Using the $\Delta\tilde{V}_{AB}$ level sets, we estimate $(\Delta\tilde{V}_{AB})_1 \approx 30$ m/s. The transfer time is approximately three Europa revolutions (around 10 days), and the new $\tilde{V}_\infty$ is around 1.6 km/s. The second VILM again consists of a gravity assist and an impulsive maneuver. The gravity assist moves the spacecraft r_a–r_p left and down on the graph until intersecting the $5{:}4^+_0$ curve (point D). The second VILM takes approximately five Europa revolutions, it costs approximately 60 m/s, and it reduces the V_∞ to less than 1.2 km/s. We design the third VILM in the same way and end up with a total transfer time of $6 + 4 + 3 = 13$ Europa revolutions and a total cost of approximately $60 + 60 + 30 = 150$ m/s, to which we can add the orbit-insertion $\Delta\tilde{V}_\pi$ for $\tilde{V}_{\infty\text{final}} = 0.8$ km/s and the desired $\tilde{h}_\pi$.

This design strategy is well-suited for a branch-and-bound search [23]: a global minimization algorithm composed of three steps. The first step (branching) splits the solution space in subsets (nodes) that are linked in a tree structure. The second step (bounding) evaluates the upper and lower bounds of the merit function for a given node. The third step (pruning) discards the nodes with lower bounds greater then a chosen pruning global variable (typically, the minimum solution). Using a recursive function, the tree can be explored efficiently because suboptimal solutions are pruned early in the search. In our problem, starting from a fixed $\tilde{V}_{\infty\text{initial}}$, the algorithm recursively applies forward exterior VILMs and stores the ToF and total cost of the endgame, which are used to prune the branches. The result of the branch-and-bound search is shown in Fig. 10, in which we plot some of the solutions (stars) and the nondominated solutions (circle). The test case explained previously is one of the nondominated solutions (the square). The branch-and-bound solutions from Fig. 10 on the right agree qualitatively with those from [24] that are found using an enumerative method based on dynamic programming principles.

Minimum and Maximum ΔV Endgame Using VILMs

In this section we use the phase-free formula introduced previously to discuss the efficiency of the endgame in terms of total ΔV. We first prove that the cost of a sequence of VILMs decreases

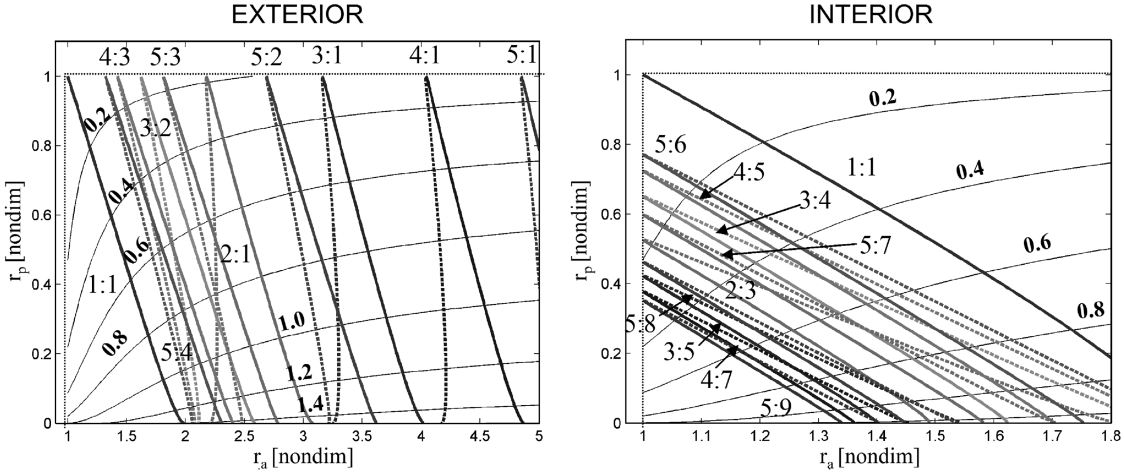

Fig. 8 Tisserand leveraging graph in nondimensional units obtained plotting the numerical solutions of the VILMs onto the Tisserand graph. Only the VILMs with $K = m - 1$ are included, as they are the most efficient. The solid thick lines are the long-transfer VILMs, and the dotted thick lines are the short-transfer VILMs. The contour lines are the V_∞ level sets.

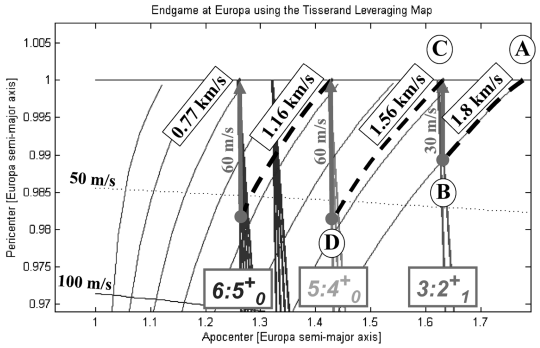

Fig. 9 Simple endgame design using the Tisserand leveraging graph. Gravity assists move the spacecraft along the V_∞ level sets. The VILMs move the spacecraft up to the $r_p = 1$ line.

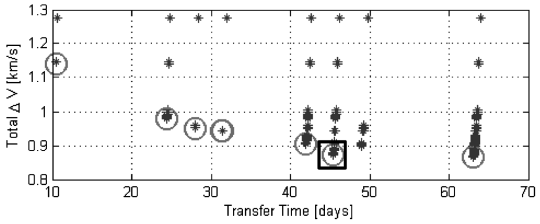

Fig. 10 Result of the branch-and-bound search for the Europa endgame problem with initial velocity of 1.8 km/s. The circles are the nondominated solutions. Among those, the square is the test case presented previously.

when favoring high-altitude gravity assist. Then we use this result to compute the minimum and maximum cost of a multiple V_∞-leveraging transfer, with a focus on the Europa endgame. Future works will include minimum-time estimates. Finally, we compute the minimum and maximum cost of a multiple V_∞-leveraging transfer between different moons, with focus on the Ganymede–Europa transfer.

Efficiency of the V_∞-Leveraging

In this section we are interested in the efficiency of the VILMs in terms of ΔV.

Theorem: The total ΔV of a sequence of VILMs decreases if one low-altitude gravity-assist VILM is replaced with two or more high-altitude gravity-assist VILMs. That is, the total ΔV of a sequence of VILMs decreases when favoring VILMs with high-altitude gravity assists.

Proof: We recall the definition of the phase-free efficiencies of Eqs. (6) and (8):

$$\epsilon_{BI-FE} \equiv \frac{\Delta V_{AB} + \Gamma}{V_{\infty H}} \qquad \epsilon_{BE-FI} \equiv \frac{\Delta V_{AB} + \Gamma}{V_{\infty L} + \Delta V_{AB}\frac{d\Gamma}{dV_{\infty L}}}$$

We recall that $\Gamma > 0$. Thus, for $\Delta V_{AB} \to 0$, $\epsilon_{BI-FE} > 0$ and $\epsilon_{BE-FI} > 0$. Now compute the variation of the efficiency due to a variation of ΔV_{AB}:

$$\frac{\partial \epsilon_{BI-FE}}{\partial \Delta V_{AB}}(\Delta V_{AB}) = \frac{V_{\infty H} - (\Delta V_{AB} + \Gamma)(D_2 V_{\infty H})}{V_{\infty H}^2}$$
$$= \frac{V_{\infty H}^2 - (\Delta V_{AB} + \Gamma)^2}{V_{\infty H}^3} = -\frac{\Gamma^2 - V_{\infty L}^2}{V_{\infty H}^2} < 0$$

$$\frac{\partial \epsilon_{BE-FI}}{\partial \Delta V_{AB}}(\Delta V_{AB}) = -\frac{\Gamma(\mathrm{d}\Gamma/\mathrm{d}V_{\infty L}) - V_{\infty L}}{(V_{\infty L} + \Delta V_{AB}(\mathrm{d}\Gamma/\mathrm{d}V_{\infty L}))^2} < 0$$

where we used $\Gamma > V_{\pi L} > V_{\infty L}$ for the first equation and $\Gamma(\mathrm{d}\Gamma/\mathrm{d}V_{\infty L}) > V_{\infty L}$ (proved in Appendix B) for the second equation. Thus, both ϵ_{BI-FE} and ϵ_{BE-FI} are positive at $\Delta V_{AB} = 0$ and strictly decreasing with ΔV_{AB}. The efficiencies are at their maximum when $\Delta V_{AB} \to 0$, i.e., for small impulsive maneuvers that (when multiple VILMs are patched together) require high-altitude gravity assist. Because this is true for any initial relative velocity, the cost of a sequence of VILMs decreases if we use more VILMs with low ΔV_{AB} as opposed to fewer VILMs with large ΔV_{AB}. In practice, flight-time consideration will limit the number of feasible VILMs.

The previous theorem is more intuitive when looking at the level sets of $V_{\infty H}(V_{\infty L}, \Delta V_{AB})$ in Eq. (4), as explained in the following.

Figure 11 shows the curves $V_{\infty H}(V_{\infty L}, \Delta V_{AB})$ for the Europa endgame case. At each gravity assist the spacecraft moves along a $V_{\infty H}$ level set. The VILM moves the spacecraft coordinates vertically from top to bottom.

The endgame discussed in the previous section and shown in Fig. 11a is composed of three VILMs for a total transfer time of 46 days and a total ΔV of 154 m/s to reduce the $\tilde{V}_\infty$ from 1.8 to 0.77 km/s. Figure 11b shows a hypothetical endgame composed of 14 VILMs, each using 10 m/s for a total of 140 m/s. The second strategy is less expensive in terms of ΔV (it certainly has a much larger transfer time), because the slope of the curves $\Delta V(V_{\infty L})$ is larger for higher ΔV. Note, in fact, that

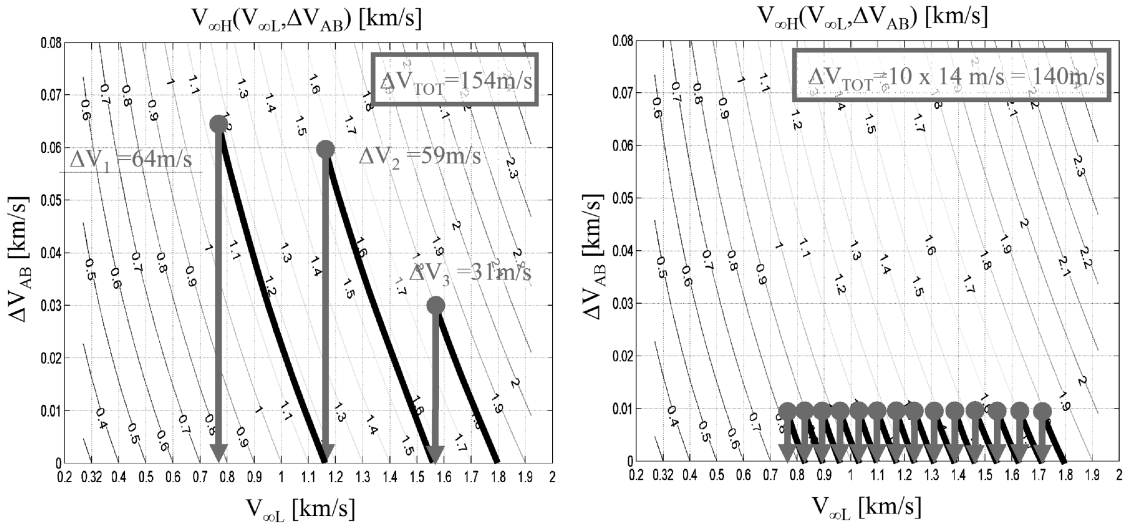

Fig. 11 Plots of a) low-altitude gravity-assist endgame and b) high-altitude gravity-assist endgame; the contour lines are level sets of $V_{\infty H}$. The cost of the high-altitude gravity-assist endgame is lower because of the slop of the level sets, which is also related to the phase-free efficiency.

$$\frac{\partial \Delta V_{AB}}{\partial V_{\infty L}} = -(\epsilon_{BE-FI})^{-1} \tag{11}$$

Thus, the least expensive way to move from an initial to a final V_∞ is by zigzagging *low* on the x axis. This suggests a simple strategy to compute the minimum ΔV of the VILM transfer, which we explain in the next section. Conversely, the more expensive way to move from an initial to a final V_∞ is to perform one large VILM.

Theoretical Minimum and Maximum ΔV for VILM Transfers with V_∞ Boundary Conditions

In this section we compute the minimum and maximum ΔV cost to transfer from a $V_{\infty H}$ to $V_{\infty L}$ through a sequence of VILMs. We also compute the minimum and maximum cost for a transfer between two minor bodies $M1$ and $M2$ (with $\tilde{a}_{(M1)} < \tilde{a}_{(M2)}$), where the boundary conditions are expressed as relative velocity at the first minor body $V_{\infty(M1)}$ and at the second minor body $V_{\infty(M2)}$ (we assume that both velocities are larger than the respective $\tilde{V}_\infty$).

In the previous section we showed that the minimum ΔV is achieved for infinite transfer times and infinite-altitude gravity assists. We recall that the linked-conics model is less and less accurate for high-altitude gravity assist, and thus we do not exclude the existence of less expensive transfers computed in more accurate models. The interested reader is referred to [4,11,13,25]. In fact, in our second paper on resonant transfers [14], we explain how the patched three-body problem allows for less expensive (even ballistic) transfers even when the VILM sequence requires a minimum ΔV of several hundred meters per second. However, less expensive transfers are at the expense of larger times of flight and larger radiation doses for missions to Europa; thus, the VILM approach and fast transfers are still used by ESA and NASA to compute the nominal trajectories to Europa and Ganymede. In this context, the theoretical minimum ΔV is a valuable piece of information during the design of resonant transfers, as it sets the limit of the VILM approach. Further, as the nondominated front in Fig. 10 on the right shows, the variation in ΔV across the full flight-time spectrum is generally not more than 10%. The minimum ΔV calculation is the main result of this paper, as it provides a simple, fast, and accurate estimate for a preliminary total ΔV cost for any moon tour.

From the previously discussed theorem, and also looking at Figs. 11 and 12, it follows that the minimum ΔV needed to transfer from two different V_∞ is the integral of the slope of the level sets $V_{\infty H}(V_{\infty L}, \Delta V_{AB})$ at $\Delta V = 0$.

From Eqs. (8) and (11) we find

$$\left.\frac{\partial \Delta V_{AB}}{\partial V_{\infty L}}\right|_{\substack{V_{\infty L}=V_\infty \\ \Delta V_{AB}=0}} = -\frac{V_\infty}{\Gamma(V_\infty)}$$

where we recall that for $V_{\infty L} = V_{\infty H} = V_\infty$ when $\Delta V_{AB} = 0$. Then the minimum cost problem between $V_{\infty L}$ and $V_{\infty H}$ is reduced to simple quadrature:

$$\Delta V^{(E,I)}_{\min}(V_{\infty L}, V_{\infty H}) = \int_{V_{\infty L}}^{V_{\infty H}} \frac{V_\infty}{\Gamma^{(E,I)}(V_\infty)}\, \mathrm{d}V_\infty \tag{12}$$

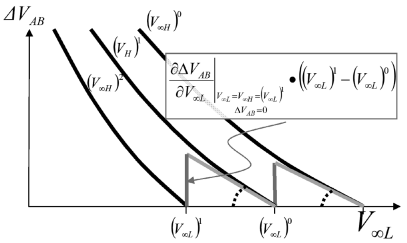

Fig. 12 Slope of the $V_{\infty H}$ level sets at $\Delta V_{AB} = 0$ can be used to estimate the ΔV_{AB} for a sequence of VILMs between infinitesimally close V_∞'s.

Using the definition of Γ in Eq. (A9), we rewrite Eq. (12) as

$$\Delta V^{(E,I)}_{\min}(V_{\infty L}, V_{\infty H}) = \int_{V_{\infty L}}^{V_{\infty H}} \frac{V_\infty^3 \pm 3V_\infty^2 + V_\infty \mp 1}{V_\infty^3 \pm 3V_\infty^2 - V_\infty \mp 7}\, \mathrm{d}t \tag{13}$$

where the integral can be solved numerically with quadrature or with partial fractions. We recall that $0 \le V_\infty \le \sqrt{2} - 1$ for the exterior VILM and $0 \le V_\infty \le 1$ for the interior VILM.

The maximum ΔV is obtained by performing one unique VILM connecting $V_{\infty H}$ and $V_{\infty L}$, and the formula is given by Eq. (5):

$$\Delta V_{\max}(V_{\infty L}, V_{\infty H}) = -\Gamma + \sqrt{\Gamma^2 + (V^2_{\infty H} - V^2_{\infty L})} \tag{14}$$

Note that $\Delta V_{\max} = V_{\infty H}$ if $V_{\infty L} = 0$. Using Eqs. (13) and (14) we can compute the minimum and maximum ΔV to increase or reduce the V_∞ using a sequence of exterior or interior VILMs. Additional details can be found in Campagnola and Russell [26].

Now we compute the minimum ΔV for transfers between two minor bodies $M1$ and $M2$ (with $\tilde{a}_{(M1)} < \tilde{a}_{(M2)}$). $\tilde{V}_{\infty(M2)}$ is the initial velocity relative to the outer minor body $M2$, and $\tilde{V}_{\infty(M1)}$ is the final velocity relative to the inner minor body $M1$. We define $\tilde{V}^{(h)}_{\infty(M1)}$ and $\tilde{V}^{(h)}_{\infty(M2)}$ as the (dimensional) relative velocities at $M1$ and $M2$ of the Hohmann transfer between the two minor bodies. We can use the scale factors associated with $M1$ and $M2$, respectively, to compute

$$V^{(h)}_{\infty(M1)} = \sqrt{\frac{2a_{M2}}{1 + a_{M2}}} - 1 \qquad V^{(h)}_{\infty(M2)} = 1 - \sqrt{\frac{2a_{M1}}{a_{M1} + 1}} \tag{15}$$

The Tisserand graph in Fig. 13a shows that the transfer is free if the initial and final relative velocities ($\tilde{V}_{\infty(M2)}$ and $\tilde{V}_{\infty(M1)}$, respectively) are greater than the Hohmann transfer relative velocities ($\tilde{V}^{(h)}_{\infty(M1)}$ and $\tilde{V}^{(h)}_{\infty(M2)}$, respectively). Figure 13a also suggests that the logical strategy for the minimum ΔV transfer consists of a sequence of interior VILMs at $M2$, followed by the Hohmann transfer, and finally a sequence of exterior VILM at $M1$. Then $\Delta V_{\min}$ is computed by applying Eq. (13) twice, first from $V_{\infty H} = V_{\infty(M2)}$ to $V_{\infty L} = V^{(h)}_{\infty(M2)}$ and then from $V_{\infty H} = V^{(h)}_{\infty(M1)}$ to $V_{\infty L} = V_{\infty(M1)}$. The $\Delta V_{\max}$ is then computed using Eq. (14) instead of Eq. (13).

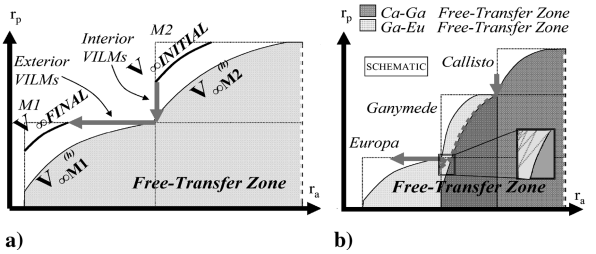

Fig. 13 Minimum VILM a) moon-to-moon transfer and b) multimoon transfer.

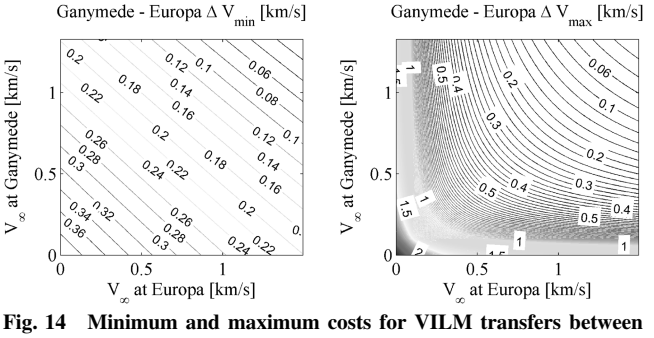

Fig. 14 Minimum and maximum costs for VILM transfers between Ganymede and Europa with V_∞ boundary conditions. The contour lines are the total ΔV level sets in km/s.

Table 1 Minimum and maximum $\Delta\tilde{V}$ for transfers between moons using VILMs.

			$\Delta V_{\min}$, km/s				Est. ToF(d) and ΔV, km/s		
Transfer	$\Delta V_{\min}$, km/s	$\Delta V_{\max}$, km/s	ΔV_{esc}	ΔV_{beg}	ΔV_{end}	ΔV_{cap}	No. VILM	$\text{ToF}_{\min}$	ΔV
Callisto–Ganymede	1.81	2.13	0.73	0.13	0.13	0.81	4	255	2.08
Callisto–Europa	1.94	3.75	0.73	0.3	0.31	0.59	11	318	2.24
Callisto–Io	2.43	6.00	0.73	0.46	0.48	0.75	23	363	2.78
Ganymede–Europa	1.71	2.18	0.82	0.14	0.16	0.59	4	151	1.98
Ganymede–Io	2.3	4.38	0.82	0.36	0.37	0.75	11	165	2.67
Europa–Io	1.76	2.54	0.6	0.21	0.2	0.75	6	126	2.05
Titan–Rhea	1.15	2.19	0.64	0.15	0.18	0.18	41	758	1.31
Titan–Dione	1.28	3.33	0.64	0.23	0.27	0.14	435	3394	1.45
Titan–Tethys	1.37	4.31	0.64	0.29	0.33	0.11	NaN	NaN	NaN
Titan–Enceladus	1.43	5.27	0.64	0.33	0.4	0.06	NaN	NaN	NaN
Reah–Dione	0.52	1.12	0.18	0.10	0.10	0.14	16	578	0.59
Reah–Tethys	0.66	2.3	0.18	0.19	0.19	0.11	225	1973	0.73
Reah–Enceladus	0.78	3.53	0.18	0.27	0.27	0.06	NaN	NaN	NaN
Dione–Tethys	0.42	0.97	0.14	0.08	0.09	0.11	20	608	0.48
Dione–Enceladus	0.55	2.19	0.14	0.17	0.18	0.06	1315	8201	0.60
Tethys–Enceladus	0.34	1.00	0.11	0.08	0.09	0.06	92	1561	0.38

Figure 13b shows that other minor bodies can be used to decrease the total $\Delta\tilde{V}$. In the case of a transfer from Callisto to Europa using Ganymede, for example, we only need to increase the initial $\tilde{V}_{\infty(Ca)}$ until $\tilde{V}^{(h)}_{\infty(Ca)}$ to reach the free-transfer zone. Then gravity assists at Ganymede, Europa, and Callisto can move the spacecraft to $\tilde{V}^{(h)}_{\infty(Eu)}$, where we start using VILMs at Europa until reaching the desired $\tilde{V}_{\infty(Eu)}$.

Using this notion, together with Eqs. (13–15), we can compute the minimum and maximum $\Delta\tilde{V}$ for any VILM transfer. We apply these formulas for a transfer between Europa and Ganymede, and plot the results in Fig. 14.

Theoretical Minimum and Maximum $\Delta\tilde{V}$ for Transfers with h_π Boundary Conditions

In this section we compute the $\Delta\tilde{V}$ for a sequence of VILMs connecting a circular orbit at $M1$ with a circular orbit at $M2$. Pushing the VILM model to its limit, we start considering $r_\pi \to \infty$. In this case V_c, $\bar{V}_\infty$, V_π, $V_{\infty L} \to 0$, and the maximum ΔV are given by formula (14), which also corresponds to the cost of a Hohmann transfer ΔV when no VILM is implemented. In general, we consider the Hohmann transfer as the $\Delta V_{\max}$ to transfer from given circular orbits.

The minimum cost is computed using Eq. (13). In particular, the cost to reach the $\tilde{V}^{(h)}_{\infty(M1)}$ and $\tilde{V}^{(h)}_{\infty(M2)}$ in the $M1$ and $M2$ non-dimensional units are

$$\Delta V_{(Mi)}(V_{c(Mi)}) = \bar{V}_{\pi(Mi)}(V_{c(Mi)}) - V_{c(Mi)} + \int_{\tilde{V}_{\infty(Mi)}(V_{c(Mi)})}^{V^{(h)}_{\infty(Mi)}} \frac{V_\infty}{\Gamma}\, \mathrm{d}V_\infty \qquad i = 1, 2 \tag{16}$$

The first two terms on the right-hand side of Eq. (16) represent a propulsive maneuver at pericenter of the escape or insertion hyperbola. This maneuver is the escape or capture orbit-insertion maneuver (ΔV_{escape} or $\Delta V_{\text{capture}}$) required to reach the $\bar{V}_\infty$ (the minimum V_∞ at which it becomes efficient to start using VILM). The integral term represents the minimum endgame or begin-game ($\Delta V_{\text{endgame}}$ or $\Delta V_{\text{begingame}}$) to reach the Hohmann transfer conditions. Note that the total cost is a function of V_c, i.e., of the altitudes h_π.

The total minimum cost in dimensional units is

$$\Delta\tilde{V} = \Delta V_{(M1)}\tilde{V}_{M1} + \Delta V_{(M2)}\tilde{V}_{M2}$$

Table 1 shows the minimum and maximum $\Delta\tilde{V}$ (km/s) for transfers between moons in the Jupiter system and in the Saturn system. All the initial and final circular orbits are at 100 km altitude, except for the orbits at Titan, which are at 1500 km altitude. The minimum $\Delta\tilde{V}$ consists of a $\Delta\tilde{V}_{\text{escape}}$, $\Delta\tilde{V}_{\text{begingame}}$, $\Delta\tilde{V}_{\text{endgame}}$, and $\Delta\tilde{V}_{\text{capture}}$. The maximum $\Delta\tilde{V}$ is the cost of the Hohmann transfer without VILMs. In the estimated transfer time (see next section), NaN (not a number) indicates a flight time greater than 25 years. Note that by using multibody dynamics, it is possible to find long transfers that require lower $\Delta\tilde{V}$ than the one in Table 1. Also, in transfers involving low-mass flyby bodies or large separation distances, shorter flight-time solutions are possible if considering the non-tangent class of VILMs.

Table A1 shows the same results for transfers with intermoon gravity assists. In this case the cost of the transfer is significantly reduced, because the spacecraft only needs to reach the closest moons, where it can start performing several gravity assists at different moons, as explained previously and suggested in Fig. 13b.

Table A2 shows the semimajor axis and physical data[‡] used in the computation of the minimum $\Delta\tilde{V}$. We also show the radius of the circular orbits, and the corresponding $\tilde{\bar{V}}_\infty$ in case of exterior and interior VILMs. The velocity of the moon $\tilde{V}_M$ is the scale factor for all the velocities. More examples can be found in Campagnola and Russell [26].

Minimum Flight-Time Estimates

We use the synodic period between the flyby body and the spacecraft orbit to estimate minimum flight times possible between successive flybys of a single VILM. The equations giving the minimum-time estimates for a single VILM are

$$\text{ToF}_{\min} = \max(SP, T_{s/c}) \tag{17}$$

where

$$T_{s/c} = 2\pi\sqrt{a^3_{s/c}} \qquad SP = \left|\frac{2\pi}{1 - 2\pi/T_{s/c}}\right|$$

$$a_{s/c} = \begin{cases} (1 + r_a)/2 & \text{exterior} \\ (r_p + 1)/2 & \text{interior} \end{cases}$$

Unlike the $\Delta V_{\min}$ derived earlier, the $\text{ToF}_{\min}$ is only an estimate and is based on a phase-free heuristic argument that the first opportunity for a successive flyby will occur after a single synodic period between the spacecraft and the flyby body. In the synodic system, a distant flyby occurs every synodic period, whereas in reality, the close flyby (or intercept in the patched-conics model) may not occur for several synodic periods, depending on the actual intended resonance. For example, a spacecraft on a 5:6 (n:m) interior resonance will reencounter the flyby body after one synodic period (five body periods, six spacecraft periods), whereas 5:7 and 5:8 resonances will reencounter after two and three synodic periods, respectively, and so on. In general, the first true encounter will occur

[‡]Data available online at http://ssd.jpl.nasa.gov/ [retrieved Dec. 2008].

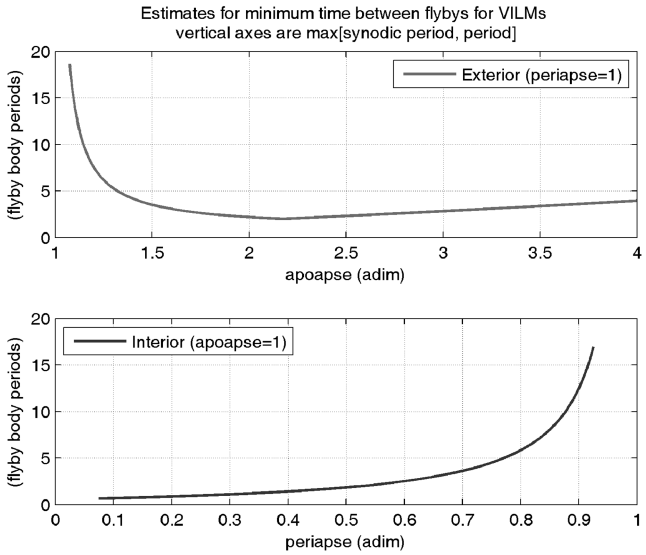

Fig. 15 Single VILM minimum-time estimates.

after $|m-n|$ synodic periods. In the unusual case in which the spacecraft period is large (exterior case, $r_p = 1$ and $r_a > 2.175$), the synodic period is smaller than one single period of the spacecraft; therefore, we put the floor of the minimum-time estimate as a single spacecraft period (assuming the m:1 resonance). Figure 15 gives the estimates [from Eq. (17)] for the exterior and interior cases as a function of pericenter and apocenter, respectively.

The minimum-time estimates therefore assume that the minimum-time VILM sequence will consist of only n:1 and n:$(n-1)$ resonances in the exterior case and only n:$(n+1)$ resonances in the interior case. These resonant structures naturally result when performing point designs of VILM sequences. An example minimum-time exterior resonance hopping sequence might consist of

$$\{(4{:}1), (3{:}1), (2{:}1), (3{:}2), (5{:}4), (8{:}9)\}$$

and an example interior minimum-time sequence is

$$\{(1{:}2), (2{:}3), (4{:}5), (7{:}8), (13{:}14)\}$$

For the minimum-time estimates, although the spacecraft (in the phase-fixed problem) may not be exactly on an n:$(n-1)$ or n:$(n+1)$ resonance, we assume that the encounter will occur after just a single synodic period (or a single spacecraft period, whichever is greatest). This phase-free assumption allows us to sum the minimum times for a sequence of VILMs together. We further assume that each patching flyby (except the last) consists of the lowest-radius flyby allowed. We conjecture therefore that this sequence with the fewest flybys possible will (approximately) lead to the lowest total flight time. Note that the time between the flybys is already approximately minimized according to phase-free (single synodic period) assumption.

We emphasize that the VILMs considered in this paper assume that 1) departure or arrival velocities are tangent to the flyby body and 2) propulsive maneuvers occur at apses and tangent to the velocity. A broader class of (ΔV-suboptimal but potentially ToF-optimal) VILMs exist without these constraints. In cases in which the flyby body is incapable of providing large gravity assist ΔV, fewer flybys may be required to hop between resonances if the broader class of nontangent VILMs are considered. Note that the minimum-time strategy outlined here is based on the tangent VILMs only. Future works will consider the nontangent cases and how these impact minimum flight-time solutions.

The minimum-time strategy for sequences of tangent VILMs is evaluated for each of the moon pairs given in Table 1, assuming the same boundary conditions on V_∞ as used in the minimum ΔV. The approximate minimum time and associated ΔV (including capture and escape) and total number of required VILMs for the full sequence are reported. The moon pairs with very small masses and or large separation distances require very long flight times and hundreds or thousands of tangent VILMs to complete. In these cases, nontangent

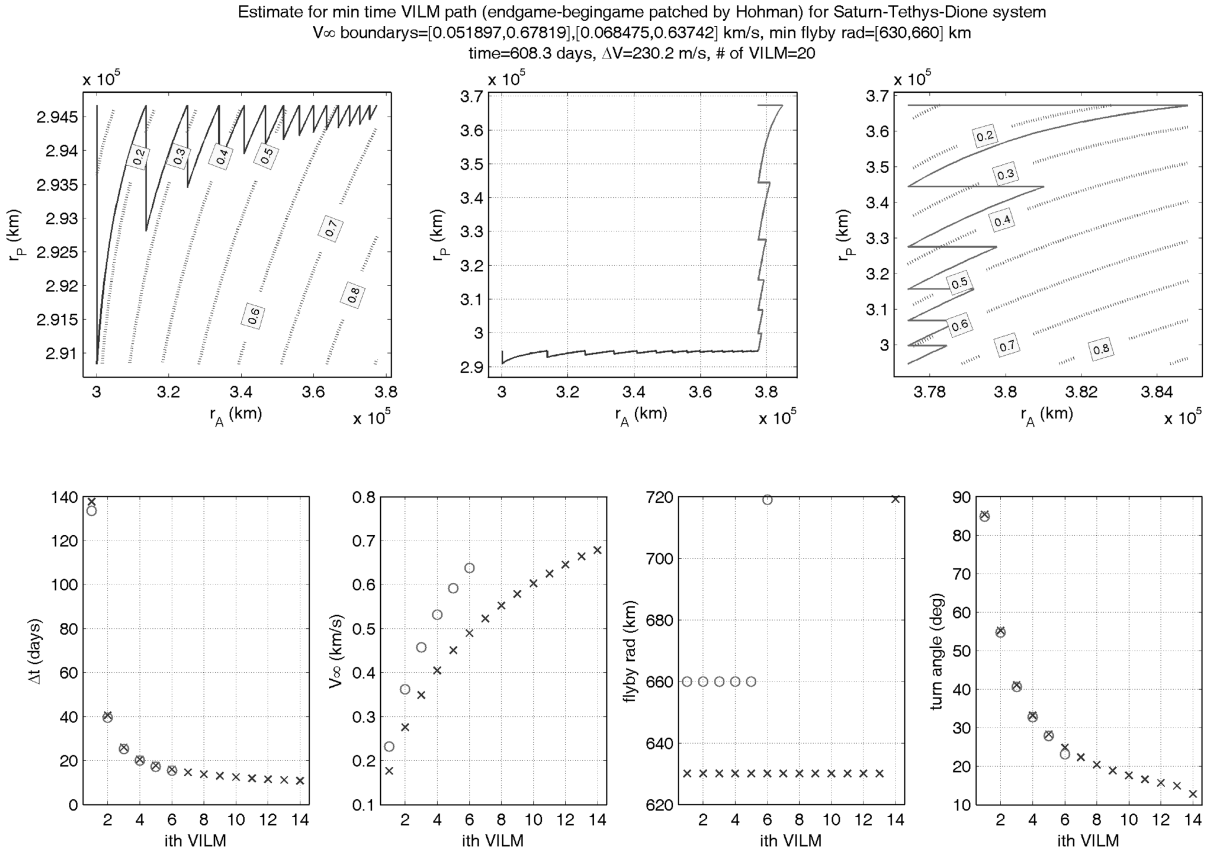

Fig. 16 Dione–Tethys minimum-time estimate VILM sequence details (from Table 1).

VILMs or other propulsive means are necessary for practical consideration. Figure 16 gives detailed information on the full sequences for the Dione–Tethys example.

Conclusions

In this paper new formulas for the V_∞-leveraging maneuver (VILM) are presented. We use these formulas to show that the VILM is only efficient when the V_∞ is larger than a minimum value. We also use the formulas to build a new graphical tool, the leveraging graph, which gives insight into the VILM problem and allows for a fast, intuitive, and preliminary design of VILM transfers. The analysis of the VILM efficiency reveals that the total ΔV of a sequence of VILMs decreases when implementing high-altitude gravity assists. This suggests a simple way to compute the theoretical minimum ΔV to transfer a spacecraft between arbitrary initial conditions using sequences of VILMs. The minimum ΔV is found by solving a simple quadrature formula. We use this formula to compute the minimum ΔV for different transfers between the Jupiter or Saturn moons. This new design capability is the main result of the paper. The leveraging graphs and associated formulas provide for a fast, accurate method for estimating flight time and ΔV trades on the complex endgame and general multimoon tour problems.

Appendix A: Derivation of the Phase-Free Formula

From Fig. 2 we see that

$$V_L = 1 \pm V_{\infty L} \rightarrow V_{\infty L}^2 = (V_L - 1)^2 \tag{A1}$$

$$V_B = V_A \mp \Delta V_{AB} \rightarrow V_B^2 = V_A^2 + (\Delta V_{AB})^2 \mp 2V_A \Delta V_{AB} \tag{A2}$$

with the upper sign referring to the exterior V_∞-leveraging, and the lower sign referred to the interior V_∞-leveraging. The velocity of the moon is $V_M^2 = k_P/a_M$. We start considering the leg L–A (the dashed lines in Fig. 2).

From the vis-viva equation $\frac{1}{2}V_L^2 - 1 = -1/(1 + r_a)$, we obtain

$$r_A = \frac{V_L^2}{2 - V_L^2} \tag{A3}$$

Note that

$$\frac{\mathrm{d}r_A}{\mathrm{d}V_L} = \frac{4V_L^2}{(V_L^2 - 2)^2} = \frac{4r_A^2}{V_L^3} \tag{A4}$$

and

$$\frac{1}{r_A} = \frac{2}{V_L^2} - 1 \tag{A5}$$

From the conservation of the energy and momentum, respectively, we have

$$\frac{1}{2}V_L^2 - 1 = \frac{1}{2}V_A^2 - \frac{1}{r_A} \rightarrow 2\left(1 - \frac{1}{r_A}\right) = V_L^2 - V_A^2 \tag{A6}$$

$$V_A = \frac{V_L}{r_A} \tag{A7}$$

Using Eq. (A5), we have

$$V_A = \frac{2 - V_L^2}{V_L} \tag{A8}$$

We now use r_A in Eq. (A3), V_A in Eq. (A8), and V_L in Eq. (A1) to define

$$\begin{aligned}\Gamma(V_{\infty L}) &\equiv \pm(r_A - V_A) = \pm\left(\frac{V_L^2}{2 - V_L^2} - \frac{2 - V_L^2}{V_L}\right) \\ &= V_{\infty L}\frac{V_{\infty L}^3 \pm 3V_{\infty L}^2 - V_{\infty L} \mp 7}{V_{\infty L}^3 \pm 3V_{\infty L}^2 + V_{\infty L} \mp 1}\end{aligned} \tag{A9}$$

Note that Γ is positive, monotonic strictly increasing function of $V_{\infty L}$ because $\Gamma(0) = 0$ and

$$\begin{aligned}\frac{\mathrm{d}\Gamma}{\mathrm{d}V_{\infty L}} &= \pm\frac{\mathrm{d}\Gamma}{\mathrm{d}V_L} = \frac{\mathrm{d}(r_A - V_L/r_A)}{\mathrm{d}V_L} = \frac{\mathrm{d}r_A}{\mathrm{d}V_L}(1 + V_L/r_A^2) - \frac{1}{r_A} = \frac{4r_A^2}{V_L^3} \\ &+ \frac{4}{V_L^2} - \frac{2}{V_L^2} + 1 = \frac{4r_A^2}{V_L^3} + \frac{2}{V_L^2} + 1 > 0\end{aligned} \tag{A10}$$

Now we consider the leg H–B.

Considering the triangle composed by V_M, $V_{\infty H}$, and V_H in Fig. 1 and using the conservation of momentum,

$$V_{\infty H}^2 = 1 + V_H^2 - 2V_H \cos\gamma = 1 + V_H^2 - 2V_B r_A \tag{A11}$$

From the conservation of the energy and from Eq. (A6),

$$V_H^2 - V_B^2 = 2\left(1 - \frac{1}{r_A}\right) = V_L^2 - V_A^2 \rightarrow V_H^2 = V_L^2 + V_B^2 - V_A^2 \tag{A12}$$

From combining Eqs. (A11) and (A12), we get

$$\begin{aligned}V_{\infty H}^2 &= 1 + V_B^2 - V_A^2 + V_L^2 - 2V_B r_A = 1 + (\Delta V_{AB})^2 \mp 2V_A \Delta V_{AB} \\ &+ V_L^2 - 2V_A r_A \pm 2\Delta V_{AB} r_A = 1 + V_L^2 - 2V_L + (\Delta V_{AB})^2 \\ &\pm 2\Delta V_{AB}(r_A - V_A) = V_{\infty L}^2 + (\Delta V_{AB})^2 \pm 2\Delta V_{AB}(r_A - V_A)\end{aligned} \tag{A13}$$

Using the function Γ defined in Eq. (A9), we finally get

$$V_{\infty H}^2 = V_{\infty L}^2 + \Delta V_{AB}^2 + 2\Delta V_{AB}\Gamma$$

and also

Table A1 Minimum $\Delta\tilde{V}$ for transfers between moons using VILMs and gravity assists[a]

Transfer	$\Delta V_{\min}$, km/s	$\Delta V_{\max}$, km/s	$\Delta V_{\min}$, km/s			
			ΔV_{esc}	ΔV_{beg}	ΔV_{end}	ΔV_{cap}
Callisto–G-Europa	1.61	2.07	0.73	0.13	0.16	0.59
Callisto–G-E-Io	1.81	2.35	0.73	0.13	0.2	0.75
Ganymede–E-Io	1.91	2.45	0.82	0.14	0.2	0.75
Titan–R-Dione	1.03	1.55	0.64	0.15	0.099	0.14
Titan–R-D-Tethys	0.98	1.47	0.64	0.15	0.086	0.11
Titan–R-D-T-Enceladus	0.93	1.5	0.64	0.15	0.086	0.061
Reah–D-Tethys	0.47	1.04	0.18	0.097	0.086	0.11
Reah–D-T-Enceladus	0.43	1.07	0.18	0.097	0.086	0.061
Dione–T-Enceladus	0.37	1	0.14	0.084	0.086	0.061

[a]The minimum $\Delta\tilde{V}$ is computed assuming infinite transfer time. The maximum $\Delta\tilde{V}$ is the cost of the Hohmann transfers to the closest inner/outer moons. Using multibody dynamics it might be possible to find long transfers that require lower $\Delta\tilde{V}$ than the one in this table.

Table A2 Moon data used for the computation of the ΔVs and transfer times

Moon	$\tilde{\mu}_M$, km^3/s^2	$\tilde{a}_M$, km	$\tilde{V}_M$, km/s	$\tilde{r}_\pi$, km	$\tilde{\tilde{V}}_\infty(\tilde{r}_\pi)$ E/I, km/s
Io	5960	421,800	17.330	1922	0.351/0.368
Europa	3203	671,100	13.739	1661	0.277/0.290
Ganymede	9888	1,070,400	10.879	2731	0.372/0.404
Callisto	7179	1,882,700	8.203	2510	0.328/0.361
Enceladus	7	238,040	12.624	352	0.029/0.029
Tethys	41	294,670	11.346	633	0.052/0.052
Dione	73	377,420	10.025	662	0.067/0.068
Rhea	154	527,070	8.484	864	0.085/0.087
Titan	8978	1,221,870	5.572	4076	0.283/0.321

$$\Delta V_{AB} = -\Gamma + \sqrt{\Gamma^2 + (V_{\infty H}^2 - V_{\infty L}^2)}$$

Note that we exclude the negative root, as ΔV_{AB} has to be positive.

Appendix B: Sign of $\Gamma(\mathrm{d}\Gamma/\mathrm{d}V_{\infty L}) - V_{\infty L}$

First note that

$$\frac{\mathrm{d}\Gamma}{\mathrm{d}V_{\infty L}}\Gamma - V_{\infty L} = \frac{1}{2}\frac{\mathrm{d}(\Gamma^2)}{\mathrm{d}V_{\infty L}} - V_{\infty L} \tag{B1}$$

We recall that

$$r_A = \frac{V_L^2}{2 - V_L^2} = -\frac{2}{V_L^2 - 2} - 1 \tag{B2}$$

$$V_A = \frac{V_L}{r_A} = \frac{2}{V_L} - V_L \tag{B3}$$

So that

$$V_A^2 = V_L^2 + \frac{4}{V_L^2} - 4 = V_L^2 + 2\left(\frac{2}{V_L^2} - 1\right) - 2 = V_L^2 - 2\left(\frac{1}{r_A} - 1\right)$$

Also because

$$\frac{\mathrm{d}}{\mathrm{d}V_{\infty L}} = \pm\frac{\mathrm{d}}{\mathrm{d}V_L}$$

$$\frac{\mathrm{d}r_A}{\mathrm{d}V_{\infty L}} = \pm\frac{\mathrm{d}r_A}{\mathrm{d}V_L} = \pm\frac{2V_L}{(V_L^2 - 2)^2} \tag{B4}$$

Now let us compute

$$(\Gamma^2) = (r_A - V_A)^2 = r_A^2 + V_A^2 - 2r_A V_A = r_A^2 + V_L^2 - 2\left(\frac{1}{r_A} - 1\right)$$

$$- 2V_L = r_A^2 + \frac{2}{r_A} + (V_L - 1)^2 - 3 = r_A^2 + \frac{2}{r_A} + (V_{\infty L})^2 - 3$$

Then

$$\frac{\mathrm{d}\Gamma}{\mathrm{d}V_{\infty L}}\Gamma - V_{\infty L} = \frac{1}{2}\frac{\mathrm{d}(\Gamma^2)}{\mathrm{d}V_{\infty L}} - V_{\infty L} = \frac{1}{2}\left(2r_A - \frac{2}{r_A^2}\right)\frac{\mathrm{d}r_A}{\mathrm{d}V_{\infty L}}$$

$$+ V_{\infty L} - V_{\infty L} = \pm\frac{2V_L}{(V_L^2 - 2)^2}\left(\frac{r_A^3 - 1}{r_A^2}\right)$$

$$= \pm(r_A^3 - 1)\frac{2V_L}{(V_L^2 - 2)^2}\frac{(V_L^2 - 2)^2}{V_L^4} = |r_A^3 - 1|\frac{2}{V_L^3} > 0$$

Acknowledgments

The authors would like to thank Jon Sims [Jet Propulsion Laboratory, California Institute of Technology (JPL)], Anastassios Petropouls (JPL), Arnaud Boutonnet (ESA), Nathan Strange (JPL), and Shane Ross (Polytechnic Institute and State University) for their valuable comments.

References

[1] Johannesen, J. R., and D'Amario, L. A., "Europa Orbiter Mission Trajectory Design," *Advances in the Astronautical Sciences*, Vol. 103, Pt. 3, Univelt, San Diego, CA, 1999, pp. 895–908; also American Astronautical Society Paper 99-360.

[2] Hollenbeck, G., "New Flight Techniques for Outer Planet Missions," *AAS Microfiche Series*, Vol. 26, Univelt, San Diego, CA, 1975; also American Astronautical Society Paper 75-087.

[3] Sims, J. A., Longuski, J. M., and Staugler, A., "V-Infinity Leveraging for Interplanetary Missions: Multiple-Revolution Orbit Techniques," *Journal of Guidance, Control, and Dynamics*, Vol. 20, No. 3, 1997, pp. 409–415. doi:10.2514/2.4064

[4] Ross, S. D., and Scheeres, D. J., "Multiple Gravity Assists, Capture, and Escape in the Restricted Three-Body Problem," *SIAM Journal on Applied Dynamical Systems*, Vol. 6, No. 3, Jan. 2007, pp. 576–596. doi:10.1137/060663374

[5] Boutonnet, A., de Pascale, P., and Canalias, E., "Design of the Laplace Mission," 59th International Astronautical Congress, Paper 08-C1.6, Glasgow, Scotland, U.K., 2008.

[6] McAdams, J. V., Dunham, D. W., Farquhar, R. W., Taylor, A. H., and Williams, B. G., "Trajectory Design and Maneuver Strategy for the Messenger Mission to Mercury," *Journal of Spacecraft and Rockets*, Vol. 43, No. 5, 2006, pp. 1054–1064. doi:10.2514/1.18178

[7] Langevin, Y., "Chemical and Solar Electric Propulsion Option for a Cornerstone Mission to Mercury," *Acta Astronautica*, Vol. 47, No. 2-9, 2000, pp. 443–452. doi:10.1016/S0094-5765(00)00084-9

[8] Jehn, R., Campagnola, S., Garcia, D., and Kemble, S., "*Low-Thrust Approach and Gravitational Capture at Mercury*," ESA Special Publication for the 18th International Symposium on Space Flight Dynamics, Vol. 548, ESA Publications Div., Noordwijk, The Netherlands, 2004, p. 487.

[9] Goodson, T. D., Gray, D. L., and Hahn, Y., "Cassini Maneuver Experience: Launch And Early Cruise," AIAA Guidance, Navigation, and Control Conference, AIAA Paper 98-4224, Boston, Aug. 1998.

[10] Kowalkowski, T. D., Johannesen, J. R., and Try, L., "Launch Period Development for the Juno Mission to Jupiter," AIAA/AAS Astrodynamics Specialist Conference and Exhibit, AIAA Paper 2008-7369, Honolulu, HI, Aug. 2008.

[11] Ross, S. D., and Lo, M. W., "Design of a Multi-Moon Orbiter," *Advances in the Astronautical Sciences*, Vol. 114, Univelt, San Diego, CA, 2003, pp. 669–684; also American Astronautical Society, Paper 03-143.

[12] Schoenmaekers, J., Pulido, J., and Cano, J., "SMART-1 Moon Mission: Trajectory Design Using the Moon Gravity," ESA TR SI-ESC-RP-5501, European Space Operation Center, Darmstadt, Germany, 1999.

[13] Grover, P., and Ross, S. D., "Designing Trajectories in a Planet-Moon Environment Using the Controlled Keplerian Map," *Journal of Guidance, Control, and Dynamics*, Vol. 32, No. 2, 2009, pp. 437–444. doi:10.2514/1.38320

[14] Campagnola, S., and Russell, R. P., "Endgame Problem Part 2: Multi-Body Technique and the Tisserand–Poincaré Graph,"*Journal of Guidance, Control, and Dynamics*, Vol. 33, No. 2, March–April 2009, pp. 476–486. doi:10.2514/1.44290

[15] Sweetser, T. H., "Jacobi's Integral and DV-Earth Gravity Assist (DV-EGA) Trajectories," *Advances in the Astronautical Sciences*, Vol. 85, Univelt, San Diego, CA, 1993, pp. 417–430; also American Astronautical Society, Paper 93-635.

[16] Vasile, M., and Campagnola, S., "Design of Low-Thrust Multi-Gravity Assist Trajectories to Europa," *Journal of the British Interplanetary Society*, Vol. 62, No. 1, Jan. 2009, pp. 15–31.

[17] Abraham, R., Marsden, J. E., and Ratiu, T. S., *Manifold, Tensor, Analysis, and Applications*, Springer, New York, 1988.

[18] Labunsky, A., Papkov, O., and Sukhanov, K., *Multiple Gravity Assist Interplanetary Trajectories*, Earth Space Institute Book Series, Gordon and Breach, London, 1998, pp. 33–68.

[19] Strange, N. J., and Longuski, J. M., "Graphical Method for Gravity-assist Trajectory Design," *Journal of Spacecraft and Rockets*, Vol. 39, No. 1, 2002, pp. 9–16.
doi:10.2514/2.3800

[20] Strange, N. J., and Sims, J. A., "Methods for the Design of *V*-Infinity Leveraging Maneuvers," *Advances in the Astronautical Sciences*, Vol. 109, Univelt, San Diego, CA, 2001, pp. 1959–1976; also American Astronautical Society, Paper 01-437.

[21] Petropoulos, A. E., Longuski, J. M., and Bonfiglio, E. P., "Trajectories to Jupiter via Gravity Assists from Venus, Earth, and Mars," *Journal of Spacecraft and Rockets*, Vol. 37, No. 6, 2000, pp. 776–783.
doi:10.2514/2.3650

[22] Kahn, M., Campagnola, S., and Croon, M., "End-to-End Mission Analysis for a Low-Cost, Two-Spacecraft Mission to Europa," *Advances in Astronautical Sciences*, Vol. 119, Univelt, San Diego, CA, CA, 2004, pp. 463–472; also American Astronautical Society, Paper 132.

[23] Land, A. H., and Doig, A. G., "An Automatic Method of Solving Discrete Programming Problems," *Econometrica: Journal of the Econometric Society*, Vol. 28, No. 3, July 1960, pp. 497–520.

[24] Brinkerhoff, A. T., and Russell, R. P., "Pathfinding and *V*-Infinity Leveraging for Planetary Moon Tour Missions," AAS/AIAA Space Flight Mechanics Meeting, American Astronautical Society, Paper 09-222, Savannah, GA, Feb. 2009.

[25] Gawlik, E. S., Marsden, J. E., Campagnola, S., and Moore, A., "Invariant Manifolds, Discrete Mechanics, and Trajectory Design for a Mission to Titan," AAS/AIAA Space Flight Mechanics Meeting, American Astronautical Society, Paper 09-226, Savannah, GA, Feb. 2009.

[26] Campagnola, S., and Russell, R. P., "The Endgame Problem Part A: *V*-Infinity Leveraging Technique and the Leveraging Graph," AAS/AIAA Space Flight Mechanics Meeting, American Astronautical Society, Paper 09-224, Savannah, GA, Feb. 2009.